Bioactive Materials 48 (2025) 118–134

Contents lists available at ScienceDirect

Bioactive Materials

journal homepage: www.keaipublishing.com/en/journals/bioactive-materials

"Monitor-and-treat" that integrates bacterio-therapeutics and bio-optics for infected wound management

Longbao Feng [a,1], Qing Peng [b,1], Li Miao [c,1], Chenghao Cai [d], Franklin R. Tay [e], Shuqin Zhou [f], Ying Zhang [b], Zonghua Liu [a,**], Xingang Wang [d,***], Yang Jiao [c,****], Rui Guo [a,*]

[a] Key Laboratory of Biomaterials of Guangdong Higher Education Institutes, Guangdong Provincial Engineering and Technological Research Centre for Drug Carrie Development, Department of Biomedical Engineering, Jinan University, Guangzhou, 510632, PR China
[b] Central Laboratory of the Second Affiliated Hospital, School of Medicine, The Chinese University of Hong Kong, Shenzhen & Longgang District People's Hospital of Shenzhen, Shenzhen, 518172, PR China
[c] Department of Stomatology, The Seventh Medical Center of PLA General Hospital, Beijing, 100700, PR China
[d] Department of Burns & Wound Care Center, The 2nd Affiliated Hospital of Zhejiang University College of Medicine, Hangzhou, 310009, PR China
[e] The Graduate School, Augusta University, Augusta, GA, 30912, USA
[f] Department of Anesthesiology of the Second Affiliated Hospital, School of Medicine, The Chinese University of Hong Kong, Shenzhen & Longgang District People's Hospital of Shenzhen, Shenzhen, 518172, PR China

ARTICLE INFO

Keywords:
Multifunctional
Hydrogel
Bacterio-therapeutics
Bio-optics
Infected wound

ABSTRACT

Wound infections are one of the major threats to human health, accounting for millions of deaths annually. Real-time monitoring, accurate diagnosis, and on-demand therapy are crucial to minimizing complications and saving lives. Herein, we propose a "monitor-and-treat" strategy for infected wound management by integrating the emerging development of bacterio-therapeutics and bio-optics. The upper layer consists of gelatin methacryloyl (GelMA)-collagen III methacryloyl (Col_3MA) (GC), Reuterin (Reu) isolated from the probiotic *Lactobacillus reuteri* (L. reuteri) and microfluidic safflower polysaccharide (SPS)@GelMA microspheres using 3D printing technology. The lower layer is made of acryloylated glycine (ACG) hydrogel with tissue adhesion capability, which enables the hydrogel to adapt to the movement and stretching of the skin. By integrating temperature-sensitive polydimethylsiloxane (PDMS) optical fibers, the ACG-GC/Reu/SPS-PDMS hydrogel could accurately and steadily sense and send wound temperature information to intelligent devices for real-time monitoring of the healing status ("monitor"). The double-layered hydrogel not only inhibited bacterial survival and colonization (97.4 % against *E. coli* and 99 % against *S. aureus*), but also exhibited remarkable hemostatic properties. Furthermore, it was conducive to L929 cell proliferation and pro-angiogenesis, and promoted the polarization of pro-inflammatory M1 macrophages to the anti-inflammatory M2-phenotype, therefore creating a favorable immune microenvironment at the wound site. Animal experiments using SD rats and Bama minipigs demonstrated that this hydrogel promoted wound closure, directed polarization to M2 macrophages, alleviated inflammation, enhanced neovascularization, therefore accelerating infected wound healing ("treat"). In addition, RNA-Seq analysis revealed the mechanism of action of ACG-GC/Reu/SPS-PDMS hydrogel in modulating key signaling pathways, including down-regulation of AMPK, IL-17, and NF-κB signaling pathways, activation of NLRP3 inflammatory vesicles, and enrichment of MAPK, TGF-β, PI3K-Akt, TNF, and VEGF signaling pathways. The modulation of these signaling pathways suggests that hydrogels play an important role in the molecular mechanisms that promote wound healing and tissue regeneration. Therefore, the design of this study provides an innovative and multifunctional bandage strategy that can significantly improve pathologic diagnosis and wound treatment.

Peer review under the responsibility of KeAi Communications Co., Ltd.
* Corresponding author.
** Corresponding author.
*** Corresponding author.
**** Corresponding author.
E-mail addresses: tliuzonghua@jnu.edu.cn (Z. Liu), wangxingang8157@zju.edu.cn (X. Wang), jiaoyang1989731@163.com (Y. Jiao), guorui@jnu.edu.cn (R. Guo).
[1] These authors contributed equally to this work.

https://doi.org/10.1016/j.bioactmat.2025.02.001
Received 27 November 2024; Received in revised form 18 January 2025; Accepted 2 February 2025

1. Introduction

Skin wound repair consists of four stages: hemostasis, inflammation, proliferation, and remodeling [1]. The colonization and growth of microorganisms can lead to infections, which may significantly delay wound healing and cause tissue damage, and, in severe cases, result in systemic infections such as sepsis [2]. The presence of biofilms makes these infected wounds difficult to treat. Clinically, antibiotics are commonly used to treat such infections [3].

To prevent wound infection, beneficial bacteria or genetically engineered bacteria are introduced to help inhibit the growth of pathogenic bacteria, break down bacterial biofilms, modulate immune responses, and promote wound healing [4]. Currently, antimicrobials remain the preferred clinical strategy for treating infected wounds. A large number of antimicrobial drugs have been reported to be encapsulated in hydrogels for the preparation of antimicrobial wound dressings, including antibiotics such as amoxicillin [5], ampicillin [6], tetracycline [7], gentamicin [8], ciprofloxacin [9], sulphadoxine-pyrimethamine [10] and linezolid. However, their overuse/misuse has led to the emergence of multidrug-resistant (MDR) strains, resulting in the development of recalcitrant biofilms and chronic wounds [11]. There is no doubt that antibiotic resistance and increased bacterial resistance due to biofilms have developed into a global health crisis. Therefore, there is an urgent need for the development of novel, broad-spectrum, natural antibacterial agents with low propensity for resistance. The reuterin (Reu) system is a complex multicomponent antimicrobial system produced by Lactobacillus reuteri by metabolizing glycerol [12,13]. The system mainly consists of 3-HPA, 3-HPA dimer, 3-HPA hydrate, acrolein and 3-hydroxypropionic acid [12,14]. Reu, in general, refers to 3-HPA, because it is 3-HPA that is not only the precursor of the other components but also the main antimicrobial component of the system [12,15]. Reu can inhibit ribonucleic acid reductase activity, which in turn can interfere with bacterial DNA replication to inhibit bacterial proliferation. It is a new, broad-spectrum, effective natural antimicrobial substance that can inhibit the growth of a wide range of bacteria, with the potential to be applied in the treatment of infected wounds [12]. In addition to this, continuous, non-invasive, real-time and dynamic early monitoring and diagnosis of infected wounds is essential for wound healing [16].

Currently, marker monitoring presents important early warnings of wound infections will be a key challenge in the development of the next generation of smart dressings. Diagnostic monitoring to assess changes in the wound microenvironment, such as temperature, humidity, pH and enzymes, etc., can be used to ward off infections, shorten healing time and reduce treatment costs [17–20]. Wearable biosensors, which are currently attracting attention for their ability to quantify wound healing-related markers using techniques such as electrochemical or optical [21]. Fiber-optic wearable sensors have the advantages of high sensitivity, miniaturization, real-time monitoring, and non-invasiveness [22–24], which are especially promising for monitoring wound infections. PDMS fiber optics, usually referred to as fibers or filaments made of polydimethylsiloxane, can be used as the sensing element of fiber-optic wearable sensors for monitoring pH, temperature, and other parameters [24–26]. However, the hydrophobicity and limited mechanical strength of PDMS fiber-optic sensing fibers limit cell adhesion and growth in wounds, as well as poor adhesion to the skin, and poor adhesion to the skin resulting in unstable signals [24]. Therefore, the development of novel wound monitoring dressings with real-time monitoring, early diagnosis, and on-demand treatment functions by integrating the properties of wound dressings and fiber-optic wearable sensors has become a hot research topic in recent years.

Hydrogels with three-dimensional structured hydrophilic polymer networks are able to respond to different stimuli conditions (e.g., light, temperature, pH, and ionic strength, etc.), and thus have been used for sensing and actuation [27,28]. 3D printed hydrogel scaffolds not only have the properties of hydrogels such as high porosity, suitable pore size, and pore connectivity, but also provide a place for cell growth, proliferation, differentiation, and metabolism, and have been widely used in tissue repair [29–31]. However, there are some limitations of 3D-printed hydrogel dressings during research and clinical application, such as unsatisfactory mechanical strength [32], weak adhesion to wounds [33], and poor hemostatic effect [34]. Therefore, there is an urgent need to develop a bionic band-aid with multiple efficacies, so that it can meet the various conditions required for wound healing, and also provide a favorable environment for the healing of infected wounds with its excellent adhesion, mechanical properties and rapid hemostatic ability.

In light of the aforementioned considerations, we developed a "monitor-to-treat" double-layered hydrogel as illustrated in Scheme 1. Initially, gelatin methacryloyl (GelMA)-collagen III methacryloyl (Col_3MA) (GC)/Reu/microfluidic safflower polysaccharide (SPS) @GelMA microspheres were prepared as the upper layer using 3D printing technology. Next, the adhesive acryloylated glycine (ACG) hydrogel in the lower layer exhibited high biocompatibility and could achieve rapid wound closure. The integration of PDMS enables the hydrogel to continuously and steadily monitor the temperature of the wound state through intelligent devices. The objective of the present study was to test the hypothesis that the designed hydrogel enables real-time monitoring of the healing process and promotes infected wound healing.

2. Results and discussions

2.1. Fabrication and characterization of the hydrogels

The synthesis process of the ACG-GC/Reu/SPS-PDMS hydrogel is shown in Scheme 1A and 1B. Initially, collagen III methacryloyl (Col_3MA) and gelatin methacryloyl (GelMA) were synthesized by modifying Collagen III and Gelatin with Methacrylic anhydride (MA). As shown in Fig. 1A, the ^1H NMR spectra of Col_3MA and GelMA distinctly exhibit new acrylic acid proton peaks ($=CH_2$) at 5.3 ppm and 5.5 ppm, which correspond to the hydrogen atoms on the olefinic bond of methacrylamide linkage, verifying the successful synthesis of Col_3MA and GelMA [35,36]. By using a microfluidic device, SPS@GelMA microspheres were prepared with GelMA and SPS under UV irradiation at room temperature with lithium phenyl-2,4,6-trimethylbenzoylphosphinate (LAP) as the photoinitiator. The upper layer GC/Reu/SPS hydrogel was then prepared by radical copolymerization of Col_3MA, GelMA, Reu and SPS@GelMA microspheres using 3D printing technology. The viscoelastic properties of the hydrogels were evaluated by rheological analysis to demonstrate the stability of cross-linked networks. As shown in Fig. 1C, the energy storage modulus (G') of the hydrogels was much larger than loss modulus (G''). In addition, G' and G'' of all tested hydrogels were increased and G' of the hydrogel is consistently higher than G'' as the frequency increased in the range of 0.01–10 Hz (Fig. 1D), indicating a predominantly elastic solid phase with excellent elasticity of these hydrogels. An ideal hydrogel should possess strong mechanical properties for practical use, and maintain its shape and integrity [37] (Fig. S1). By testing the hydrogels compressive stress-strain, the maximum compressive strengths of hydrogels were 24.95 ± 2.33 kPa for GC/Reu/SPS, 73.67 ± 11.22 kPa for GC/Reu, and 75.43 ± 26.42 kPa for GC, respectively. These results indicated that the compressive strength of the hydrogels can be adjusted by adding SPS@GelMA microspheres for biomedical applications in various tissues and organs. As wound dressings, hydrogels can absorb tissue permeate and provide a moist, breathable environment for the wound. Thus, the swelling properties were tested in PBS (pH 7.4) at 37 °C, and Fig. S2 shows that the swelling degree of all hydrogels increases over time. They reach swelling equilibrium in 8 h, and then stabilize; the swelling rate does not continue to rise. This behavior was attributed to the pore size of the hydrogel. The hydrogels have a tighter grid, making it difficult for water molecules to infiltrate. This results in a

lower rate and extent of swelling [38]. The inclusion of SPS@GelMA microspheres makes the hydrogel denser, further reducing the swelling rate. Next, the cumulative release profiles of SPS from the GC/Reu/SPS hydrogel were measured. As shown in Fig. 1G, there was a sustained release with 63 % with a total of 1.51 mg of SPS released after 168 h. This characteristic is beneficial for long-term drug retention. To minimize secondary damage in surgical wounds, an ideal biomedical scaffold should degrade in sync with the tissue regeneration process. Fig. 1H illustrates the degradation performance of the GC/Reu/SPS hydrogel in PBS with or without enzyme. The weight loss curve of the hydrogel showed a high degradation rate in the first 7 days. Afterwards, the degradation rate slowed down. By 21 days, the hydrogel was completely degraded in the presence of enzyme, while the hydrogel without enzyme showed more than 90 % degradation. This indicates that the hydrogel is highly biodegradable, and responds well to the biological environment for tissue regeneration. The lower layer is made of acryloylated glycine (ACG) hydrogel, which comes from the reaction between Glycine (Gly) reacts with acryloyl chloride (AC), followed by photo-triggered covalently crosslinking. The characteristic peaks of the vinyl group from AC are visible at 6.2 ppm and 5.8 ppm in the ^{1}H NMR spectra of ACG (Fig. 1B), which is indicative of successful synthesis of ACG. Adhesive property of the hydrogel is of vital importance for promoting wound closure and healing [39]. As shown in Fig. S3, the hydrogel showed excellent adhesiveness to various substrates, including biological tissues (such as heart, lung, spleen, kidney, and liver) and glass, plastic, and metal, and the adhesive strength could support the weight of those materials. Meanwhile, as can be seen from the scanning electron microscope image of the scaffold in Fig. 1E and the appearance of the scaffold in Fig. 1F, the 3D-printed mesh scaffold presents a bilayer structure with obvious cavity structure, which is more conducive to the adhesion, growth, and division of cells, and is more conducive to the transfer of nutrients and oxygen. In addition to this we used rhodamine B to simulate the *in vitro* release behavior of reuterin in hydrogels. Fig. S4A shows the full UV absorption spectrum of rhodamine B with a maximum absorption peak at 555 nm. The *in vitro* release assay further confirmed that the drug had a good dissolution behavior in the hydrogel, with a cumulative release rate of 98.56 ± 0.31 % at 168 h (Fig. S4B).

2.2. *In vitro* antibacterial activity of the hydrogels

During wound healing, bacterial infection at the wound site often exacerbates conditions and delays healing [40,41]. Thus, antibacterial wound dressings are highly esteemed for improving the therapeutic efficacy. The researchers chose Gram-positive *Staphylococcus aureus* (*S. aureus*) and Gram-negative *Escherichia coli* (*E. coli*) for the study, which are the most common pathogens in septic wound infections. In

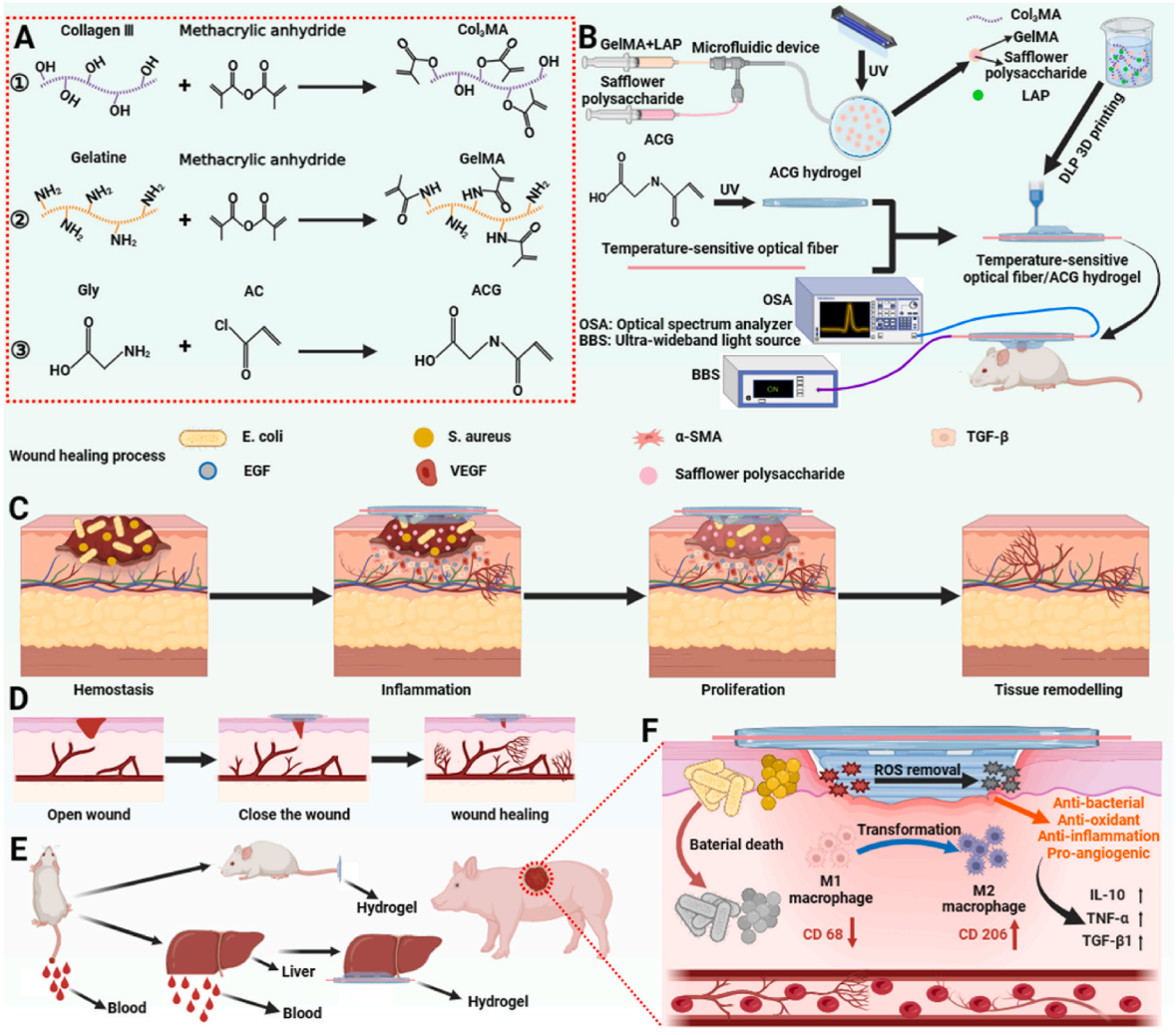

Scheme 1. Schematic illustration of the preparation and mechanism of the ACG-GC/Reu/SPS-PDMS hydrogel-based wound healing strategy.
(A) and (B) Preparation and working principle of the hydrogel; (C), (D) and (E) Application of the hydrogel for infected wound healing, wound closure and hemostasis; (F) The multifunctional hydrogel possesses antibacterial, pro-angiogenic, anti-inflammation and immunoregulatory properties for accelerating infected wound healing.

order to fully assess the antimicrobial effect, we first performed bacterial growth curve analysis and followed up with experiments when they were growing in logarithmic phase (Fig. S5A). The inhibitory effects of rhodopsin on *E. coli* and *S. aureus* were also quantitatively analyzed by determining the minimum inhibitory concentration (MIC) and minimum bactericidal concentration (MBC) of reuterin. The results showed that the MIC of reuterin was 250 μg/mL and the MBC was 1000 μg/mL for both *E. coli* and *S. aureus* (Figs. S5B and C). The antimicrobial capacity of Reu and hydrogel was evaluated using co-culture and plate counting methods (Fig. 2A). Subsequently, the antibacterial effects of Reu with different concentrations (0, 10, 100, 500 and 1000 μg/mL) against *E. coli* and *S. aureus* were examined. Results of agar plates indicated a decrease in colony number with increasing Reu concentrations; There was no colony growth at a concentration of 1000 μg/mL for both strains (Fig. S6A). Quantitative analyses of antibacterial rate revealed inhibition rates of 95.5 % for *E. coli*, and 93.1 % for *S. aureus* at 500 μg/mL (Figs. S6B and C). These rates escalated to 99.84 % and 99.97 %, respectively, when Reu concentration was increased to 1000 μg/mL. These findings inspired us to incorporate Reu into the hydrogel and explore the antibacterial activity of the hydrogel. Fig. 2B demonstrates the resultant colony growth on agar plates after co-culturing with *E. coli* and *S. aureus* across different hydrogel formulations. The sequence of colony numbers was in the order: ACG-GC/Reu/SPS < ACG-GC/Reu < ACG-GC/SPS < ACG-GC < Control. As quantified in Fig. 2C and D, the GC/Reu/SPS hydrogel had the highest antibacterial rates of 97.4 % against *E. coli*, and 99 % against *S. aureus*, respectively. Live-dead fluorescence staining was subsequently performed to examine bacterial viability (Fig. 2E). Green fluorescence indicates surviving bacteria, while red fluorescence indicates dead bacteria. *Escherichia. coli* and *S. aureus* cultured with ACG-GC/Reu/SPS and ACG-GC/Reu hydrogels predominantly displayed signs of cell death. Scanning electron microscopy observations of bacteria morphology (Fig. 2F) revealed significant structural damage and encapsulation by ruptured plasma in bacteria treated with these hydrogels. Almost all bacteria demonstrated altered or ruptured morphology and no intact bacteria was visible. These antibacterial effects are primarily attributed to the binding of Reu to bacterial ribosomes and inhibition of protein synthesis. These effects, in turn, result in disruption the biological functions of the bacteria investigated [42,43].

Bacterial biofilm formation is an important feature in bacterial infections, which not only enhances bacterial drug resistance, but also makes the infection more persistent and difficult to treat. Therefore, this study further evaluated the effectiveness of the prepared hydrogels in disrupting bacterial biofilm formation. In order to visualize the hydrogel's disrupting effect on biofilm more intuitively, a laser confocal microscope was used to image the treated bacterial biofilm. The results showed that the thickness of the bacterial biofilm in the control group increased significantly, and the bacterial aggregation was denser.

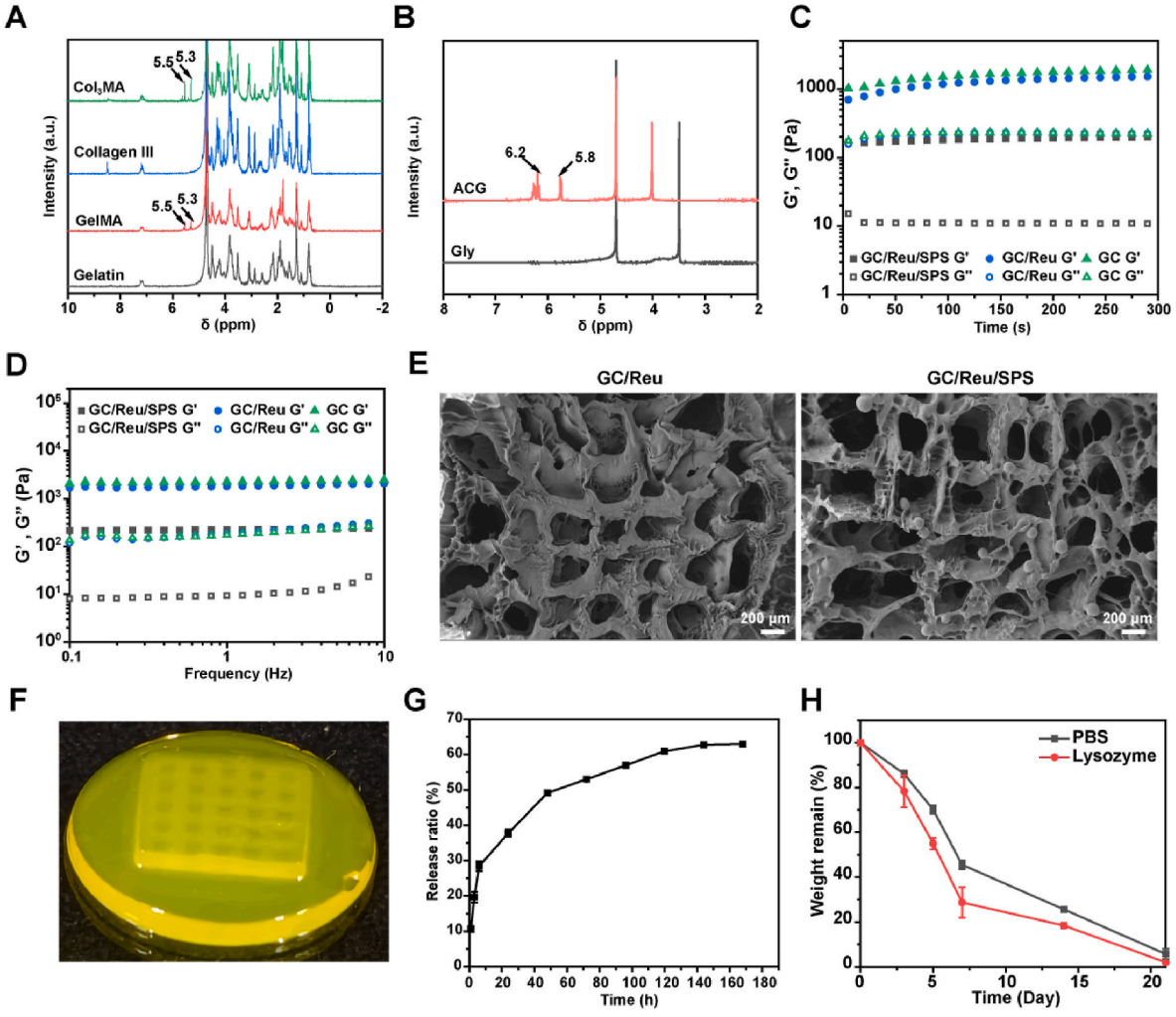

Fig. 1. Characterization of the hydrogels.
(A) and (B) ^{1}H NMR spectra of Col_3MA, Collagen III, GelMA, Gelatin, ACG and Gly; (C) and (D) Plot of hydrogel materials G′ and G″ *versus* time and *versus* frequency, respectively; (E) SEM and (F) appearance images of the hydrogels; (G) *In vitro* drug release curve of SPS from the hydrogel; (H) Degradation curves of the hydrogel.

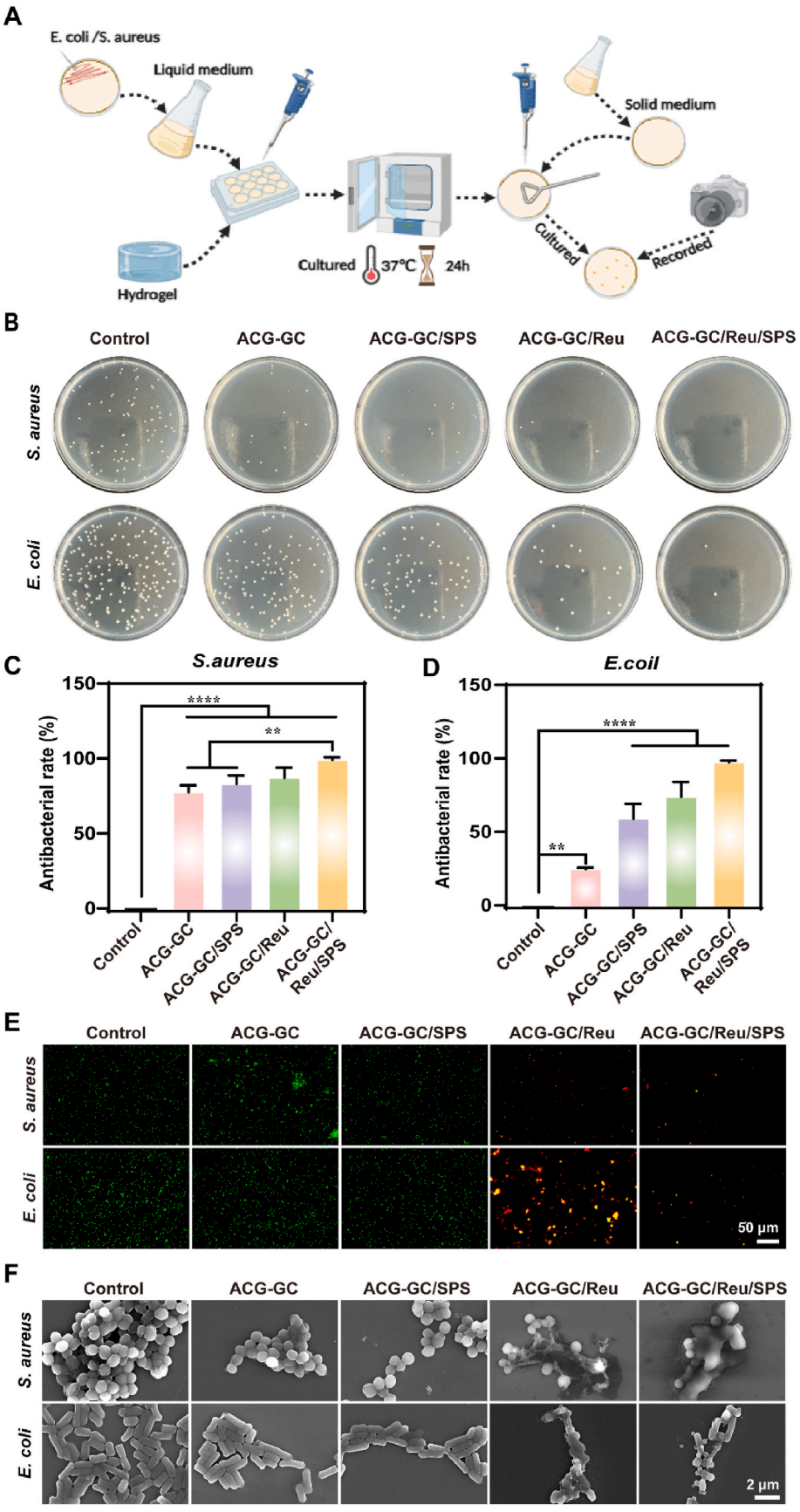

Fig. 2. *In vitro* antibacterial activity of the hydrogels.
(A) Schematic of the antibacterial experiments; (B) Agar plate images of *S. aureus* and *E. coli* colonies; (C) and (D) Antibacterial rates of the hydrogels against *S. aureus* and *E. coli*; (E) Live-dead fluorescence staining and (F) SEM images of *S. aureus* and *E. coli* cultured with the hydrogels.

Compared with the control group, the biofilm staining intensity was significantly reduced in the hydrogel group. In particular, the bacterial biofilm structure was significantly damaged in the ACG-GC/SPS/Reu hydrogel group, with less bacterial aggregation on the surface and a thinner biofilm layer formed (Fig. S7). This was mainly attributed to the unique antibacterial ability of Reu.

2.3. *In vitro* biocompatibility, pro-angiogenic and immunoregulatory effects of the hydrogel

Wound dressings interact with human tissues during use. An ideal hydrogel should exhibit low cytotoxicity to ensure safety [44]. Firstly, cell survival was analyzed with different concentrations of SPS@GelMA microspheres (0, 10, 50, 100, 200, 500 and 1000 μg/mL), which were cultured with L929 cells. The results revealed a decline in cell survival as the microsphere concentration increased (Fig. S8A). However, even at a concentration of 1000 μg/mL, the cell survival rate was still maintained above 90 %. The results indicate that SPS microspheres are non-toxic to L929 cells and have good biocompatibility. Next, biocompatibility of the hydrogel was assessed by co-culturing the extracts with L929 cells (Fig. 3A). Similar results were achieved with the CCK-8 assay after 1, 2 and 3 days of co-culture with L929 cells. Minimal cytotoxicity was

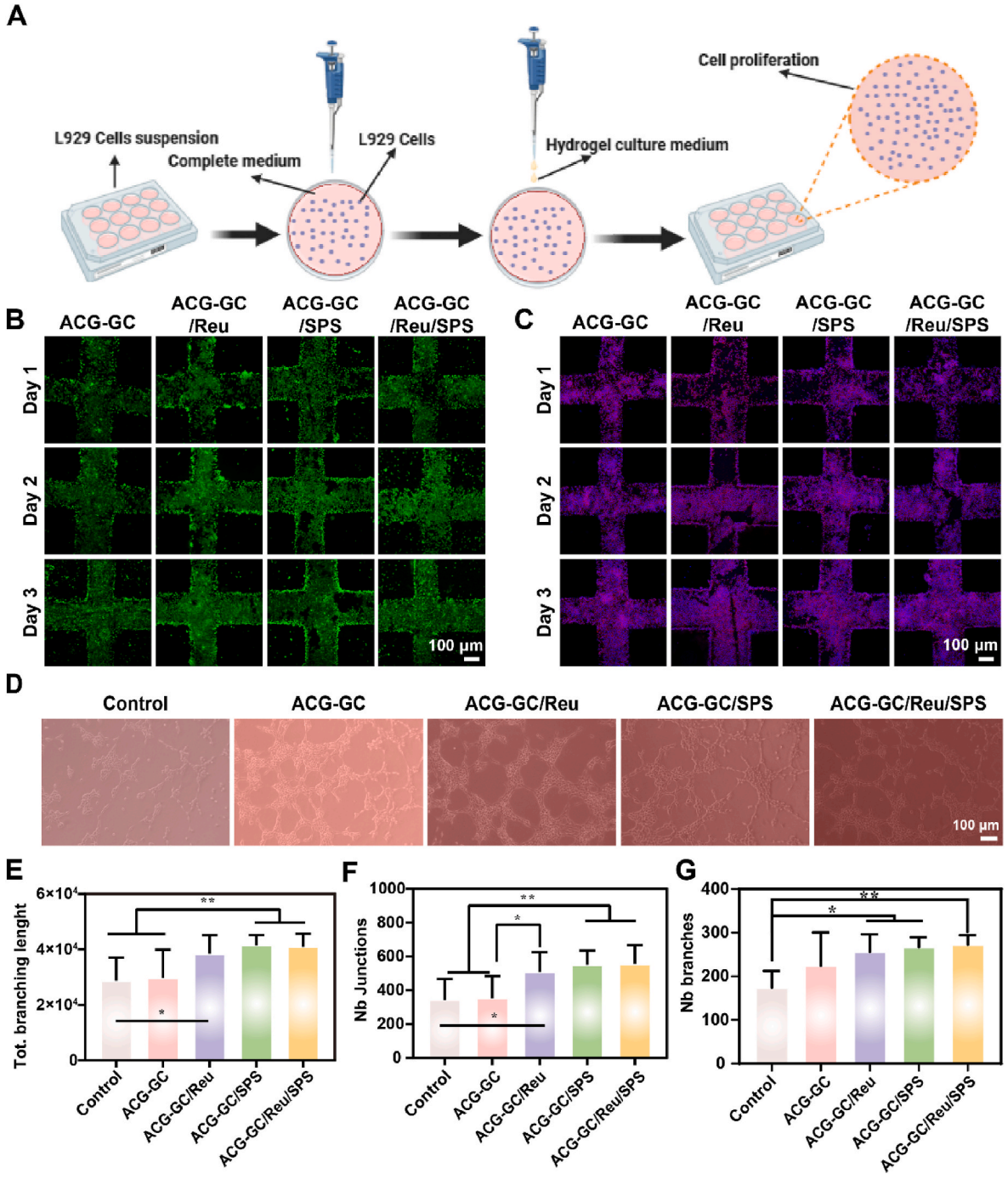

Fig. 3. *In vitro* cytocompatibility of the hydrogels.
(A) Schematic of the biocompatibility experiments; (B) Live-dead fluorescence staining images of L929 cells cultured with the hydrogels; (C) Cytoskeleton staining images of L929 cells cultured with the hydrogels; (D) Tube-forming images of HUVECs cultured with the hydrogels; Quantitative analyses of (E) total branching length, (F) total number of junctions and (G) total number of branches in angiogenic activity assays.

identified in all the hydrogel groups with cell survival rates remaining above 95 % (Fig. S8B). Next, live/dead fluorescence staining (Fig. 3B) and F-actin cytoskeleton staining (Fig. 3C) were used to investigate cell viability after 1, 2, and 3 days of culture with the hydrogel extractions. Almost all of the L929 cells were alive (green) and dead cells (red) were rarely observed in all groups. The cells exhibited healthy morphology and extended growth on the hydrogels. Angiogenesis is essential for wound repair as it provides oxygen and nutrients to the wound site and supports cytokine transport to wound healing related cells [45]. The angiogenesis potential of the hydrogel was investigated using human umbilical vein endothelial cells (HUVECs) (Fig. 3D). The total branching length, total number of junctions and total number of branches were quantified and shown in Fig. 3E–G, respectively. Both the total vessel length, the total number of junctions and the total number of branches in the ACG-GC/SPS, ACG-GC/Reu and ACG-GC/Reu/SPS groups were higher than that in the control group, with the highest values observed in the ACG-GC/Reu/SPS group. These results suggest that the presence of Reu and SPS significantly improve angiogenesis, and the ACG-GC/Reu/SPS hydrogel is advantageous for angiogenesis and tissue remolding in the infected wound site.

In this experiment, we evaluated the effects of different hydrogel treatment groups on L929 cell proliferation by Ki67 staining. The results of Fig. S9A, B showed that the Ki67 fluorescence intensity of the ACG-GC/Reu/SPS group was significantly higher than that of the other groups, indicating that the hydrogels in this group could significantly promote cell proliferation. This may be related to the synergistic effect of Reu and SPS in the hydrogels, which may enhance cell growth by promoting cell proliferation or providing a favorable microenvironment. In contrast, relatively less cell proliferation was observed in the ACG-GC and ACG-GC/Reu groups, suggesting that hydrogels containing only ACG-GC or ACG-GC/Reu components had a weaker stimulation of cell proliferation. The control group had the lowest Ki67 fluorescence intensity, indicating a lower level of cell proliferation in the absence of hydrogel treatment. This suggests that the two components of the hydrogel, Reu and SPS, may act together to accelerate tissue repair through different biological mechanisms.

In addition to this, we evaluated the effects of different hydrogel treatment groups on L929 cell migration and wound healing. By scratching experiment (Figs. S10A, B, C), the results showed that the ACG-GC/Reu/SPS group exhibited the best cell migration ability within 24 h, which significantly promoted the cells to fill the scratched area, and its healing rate was significantly higher than that of other groups. This suggests that the addition of SPS plays an important role in enhancing cell migration and healing ability. In conclusion, the ability of ACG-GC/Reu/SPS hydrogel to significantly promote the migration and wound healing of L929 cells may be closely related to its biocompatibility and the synergistic effect of Reu and SPS components, which provides a potential application in tissue repair and clinical applications.

Macrophages play a key role in tissue homeostasis, wound healing, and tissue repair [46]. These immune cells possess high plasticity and can switch polarization between two cell types (pro-inflammatory M1 phenotype macrophages and anti-inflammatory M2 phenotype macrophages) during the inflammatory response with different functions [47]. Timely M2 phenotype polarization facilitates the transition from the inflammatory stage to the remodeling stage and accelerates wound healing. However, persistent M1 macrophage polarization, and subsequent dysbalance of M1/M2 phenotype are often found at the wound site and responsible for delayed wound healing. Herein, experiments were conducted to test the hypothesis that the ACG-GC/Reu/SPS hydrogel could induce M1-to-M2 macrophage phenotype transition to alleviate inflammatory responses. Lipopolysaccharide (LPS) was used to stimulate RAW264.7 macrophages to the pro-inflammatory M1 phenotype. The expression of CD86 (M1 marker) and CD206 (M2 marker) in RAW 264.7 macrophages were assessed using flow cytometry (Fig. 4A). The relative expression levels of CD86 (Fig. S11A) and CD206 (Fig. S11B) were also quantified and statistically analyzed. The relative expression of CD86 in all the hydrogel groups was lower than that in the LPS-treated group. This trend was even more pronounced in the ACG-GC/Reu/SPS group. In contrast, the relative expression of CD206 was higher in the hydrogel groups, especially in the ACG-GC/Reu/SPS group. The M1/M2 ratio was also counted with the lowest M1/M2 ratio observed in the ACG-GC/Reu/SPS group (Fig. 4B). In addition, relative proteins were quantified with Western blotting experiments (Fig. 4E). The relative protein expression levels of CD206 and iNOS showed similar results to those derived from flow cytometry (Fig. 4C and D). These results support the hypothesis that Reu and SPS released from the ACG-GC/Reu/SPS hydrogel induce the transition of macrophages from the M1 to the M2 phenotype to improve the inflammatory microenvironment. This is crucial for promoting healing of the infected wounds.

Finally, we detected changes in the expression of pro-inflammatory and anti-inflammatory factors in RAW264.7 cells by qPCR experiments (Figs. S12A and B). The experimental results showed that compared with the control group, SPS and Reu acted together to significantly down-regulate the expression of pro-inflammatory factors TNF-α, IL-1β, and iNOS, and at the same time significantly up-regulated the expression of anti-inflammatory factors IL-10, TGF-β, and Arg-1. This shows that the synergistic effect of SPS and Reu has a significant effect in regulating macrophage M1/M2 polarization, creating an anti-inflammatory immune environment conducive to tissue regeneration. To further explore the specific signaling pathways, we detected the expression of signaling pathway proteins closely related to macrophage polarization and tissue repair using WB experiments (Figs. S13A and B). The results showed that the combined treatment of SPS and Reu inhibited the NF-κB signaling pathway (by reducing IkBα degradation), while activating the PI3K/Akt/mTOR signaling pathway. The up-regulation of ERK expression also suggested the involvement of the MAPK pathway. The combined action of these pathways may be critical for enhanced macrophage polarization, cell migration, and tissue regeneration.

2.4. *In vivo hemostatic capacity of the hydrogels*

Hemostasis plays a crucial role in the wound healing process [48]. Given the absorbent and adhesive capacities of the ACG hydrogel, we hypothesized that it should be a promising candidate for rapid hemostasis by sticking to the surrounding tissues of the bleeding point as a physical barrier. Specifically, we employed two bleeding models, including rat liver puncture wound and tail amputation models (Fig. 5). Firstly, the hemostatic capacity of the ACG hydrogel was evaluated in the liver model, which contains the most abundant blood vessels among visceral organs (Fig. 5A). Blood flowed out once the wound was created in the control group; in contrast, the areas of blood staining were smaller in the Gauze and ACG groups (Fig. 5B). In addition, the blood loss was in the following order: Control group (5.87 ± 0.36 g) > Gauze group (2.07 ± 0.47 g) > ACG group (0.20 ± 0.12 g) (Fig. 5C). The hemostasis time in the ACG group was 41.67 ± 19.8 s which was impressively less than the Control and Gauze group (Fig. 5D). Next a rat tail amputation model was used to evaluate the hemostatic property of the ACG hydrogel on massive hemorrhage (Fig. 5E). It was seen from Fig. 5F that the tail amputation model treated with the ACG-GC/Reu/SPS hydrogel bled less than the Control and Gauze groups. The quantitative results further showed that the amount of blood loss in the ACG group was 0.04 ± 0.02 g, which was significantly reduced compared to that of the Control (0.36 ± 0.07 g) and Gauze group (0.97 ± 0.3 g) (Fig. 5G) This indicated that the ACG hydrogel could reduce the blood loss by 87.7 % compared to Gauze. Furthermore, the ACG group still showed shortened blooding time (Fig. 5H). Thus, the ACG hydrogel demonstrates favorable hemostatic performance, which is primarily attributed to the adhesive property of the hydrogel. This facilitates the subsequent phases of wound healing and tissue repair [49,50].

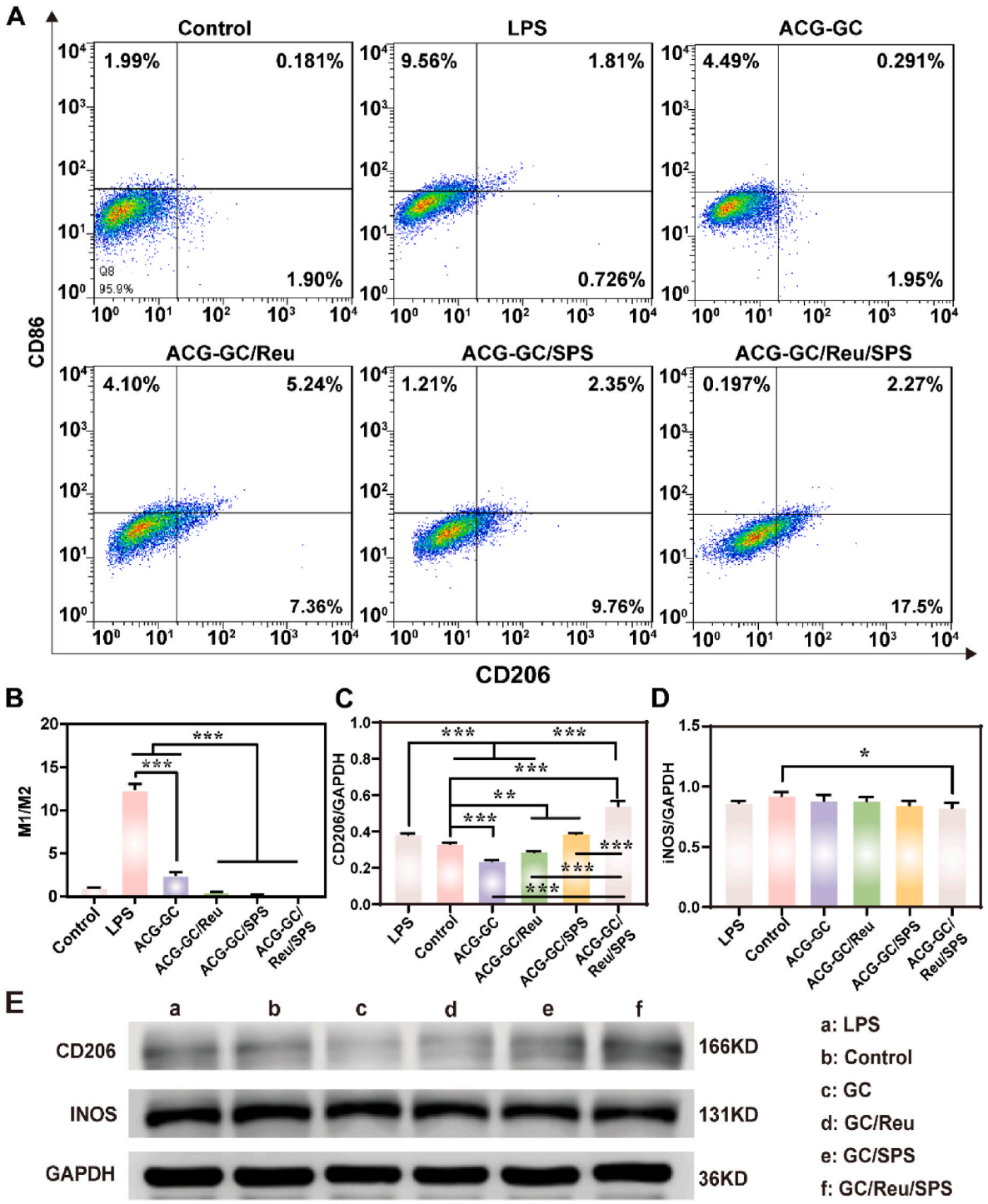

Fig. 4. ***In vitro*** **immunoregulatory property of the hydrogels.**
(A) Flow chart of fluorescent expression of CD86 and CD206 after co-culture of LPS-treated RAW264.7 cells with the hydrogel extracts; (B)Quantitative analyses of M1/M2 ratio. Quantitative analyses of (C) CD206 and (D) INOS expression. (E) Western blot images of CD206 and INOS expressions after co-culture of LPS-treated RAW264.7 cells with the hydrogel extracts.

2.5. In vivo healing capability in a total skin defect infection model of SD rats

The capacity of the ACG-GC/Reu/SPS hydrogel to promote infected wound healing was assessed in a full-thickness skin defect infection model of SD rats. The timing to apply the mixed bacterial fluid infection after successful modelling was recorded as day-1. The wounds were systematically monitored and photographed on days −1, 3, 7, 10 and 14 (Fig. 6A and B). Wound areas decreased over time in all groups after 14 days. Wounds that were covered with the ACG-GC/Reu/SPS hydrogel demonstrated accelerated wound closure. Quantitative analyses of the wound healing rates were performed (Fig. S14). Compared with the control group (16.19 ± 1.37 %), the wound healing rates were substantially higher in the GC/SPS group (31.67 ± 3.58 %), the GC/Reu group (33.60 ± 3.06 %) and the GC/Reu/SPS group (43.29 ± 1.25 %) after 3 days of treatment. In particular, the wound healing rate in the

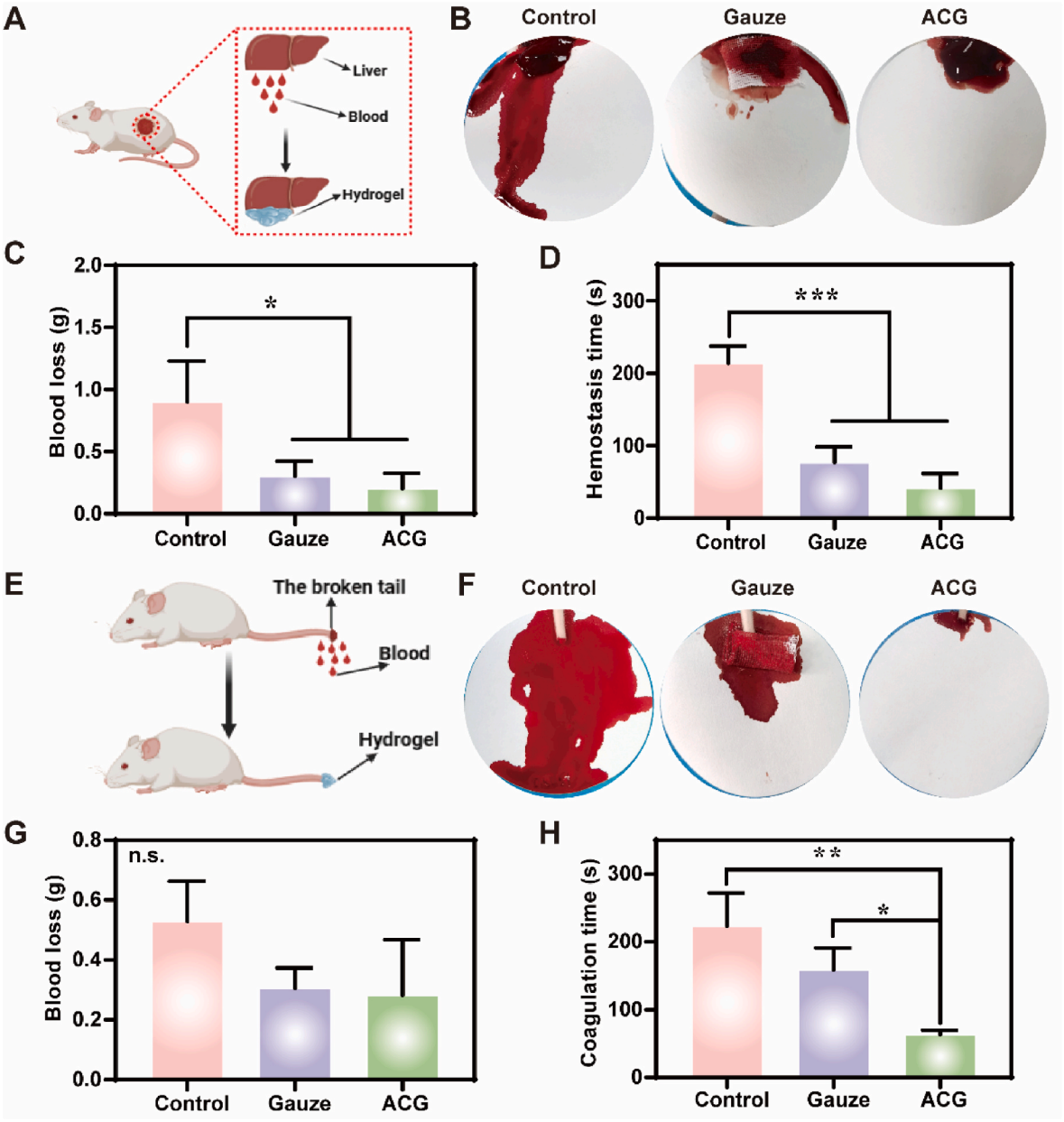

Fig. 5. ***In vivo*** **hemostatic property of the hydrogels.**
(A) Schematic of the rat liver hemostasis model; (B) Bleeding phenotype at the end of hemostasis in rat liver injury model; (C) Bleeding volume statistics of liver; (D) Quantitative analysis of hepatic hemostasis time; (E) Schematic of the rat tail amputation hemostasis model; (F) Bleeding phenotype at the end of hemostasis in rat tail amputation injury model; (G) Bleeding volume analysis of tail amputation; (H) Quantitative analysis of tail amputation hemostasis time.

GC/Reu/SPS group reached 81.09 ± 1.95 % after 7 days of treatment. This represents a significant increase compared to the other groups. After 10 days of treatment, wounds in the GC/Reu/SPS hydrogel group were essentially completely healed. This finding indicates that the hydrogel promotes wound healing more rapidly.

At the same time, we evaluated the bacterial killing effect of hydrogel on rat wounds. Fig. S15A demonstrates the growth of *E. coli* and *S. aureus* on selective media after the intervention of different hydrogel treatment groups. For *E. coli*, the ACG-GC/Reu/SPS group almost completely inhibited bacterial growth. Similarly, *S. aureus* showed significant inhibition with almost no growth in the ACG-GC/Reu/SPS group. The other hydrogel treatment groups (e.g., ACG-GC, ACG-GC/Reu, ACG-GC/SPS) inhibited bacterial growth to some extent, but not as effectively as the ACG-GC/Reu/SPS group. Fig. S15B demonstrates the quantitative statistics of the antibacterial effects of *E. coli* and *S. aureus*. The results showed that the antimicrobial rate of the ACG-GC/Reu/SPS group was significantly higher than that of the other groups, reaching 99.58 % for *E. coli* and 99.95 % for *S. aureus*, indicating that the hydrogel group was almost completely antimicrobial.

To further investigate the details of wound healing progress, hematoxylin and eosin (H&E) and Masson staining were used to stain the regenerated tissues of rats. Fig. 6C demonstrates the H&E staining, showing the healing of the wound site with a large number of inflammatory cells accumulated in the Control group 3 days after treatment. In comparison, a relatively mild inflammatory infiltrate was identified in wound tissues that were treated with the ACG-GC/Reu/SPS hydrogel. The excellent antibacterial property of the hydrogel can avoid wound infection, thus reducing the inflammatory reaction of the wound. After 14 days of treatment, the ACG-GC/Reu/SPS group showed more hair follicles and intact vascular structures. This group showed tightly

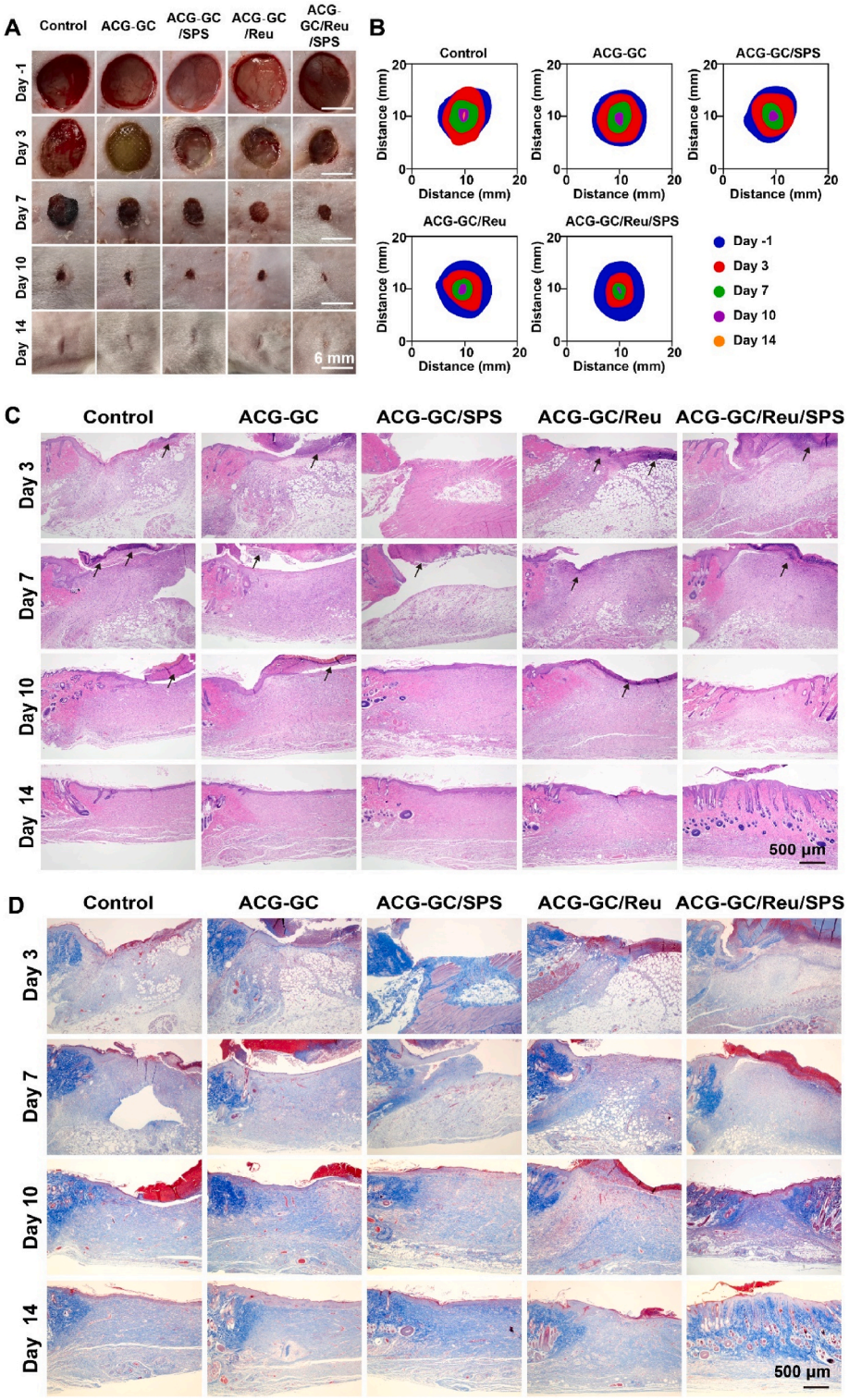

Fig. 6. *In vivo* healing capability of the hydrogels in a total skin defect infection model of SD rats.
(A) Macroscopic images of the wounds at different treatment time-points; (B) Partial wounds healed at different treatment times; (C) H&E staining and (D) Masson's trichrome staining images of the skin of the wound site after 3, 7, 10, and 14 days.

arranged granulation tissue and rejuvenated epidermal layers. As shown in Fig. 6D, Masson staining showed that all groups experienced varying degrees of collagen deposition during treatment. By day 14, wounds in the ACG-GC/Reu/SPS group exhibited the highest density of collagen deposition, and a more regularly arranged collagen fiber structure, compared to all other groups. These results strongly support that the ACG-GC/Reu/SPS hydrogel may effectively promote infected wound healing.

Immune cells such as macrophages are recruited to the wound site and generate a cascade of events that lead to the early inflammatory response. In the late stage of inflammation, M1 macrophages will polarize into the M2 phenotype to alleviate inflammation and secrete anti-inflammatory cytokines to facilitate tissue regeneration. However, persistent and severe inflammation may hinder macrophage phenotype

transition and may delay wound healing or even cause wounds to become non-healing [1]. Thus, timely switching of macrophages from the M1 to the M2 phenotype plays a vital role in tissue repair and regeneration [51]. As shown in Fig. 7A–E, the expression of TNF-α was significantly reduced after 3 and 7 days of treatment in the ACG-GC/Reu and ACG-GC/Reu/SPS groups. After treatment with the ACG-GC/Reu/SPS hydrogel, profuse TGF-β1 and IL-10 expression was observed (Fig. 7B, C, F, G). These results suggest that after 7 days of wound treatment, there was still a severe inflammatory response in both the Control and ACG-GC groups. In addition, according to the immunofluorescent staining results, the ACG-GC/Reu/SPS hydrogel had the least amount of CD68 (M1 marker) and the highest CD206 (M2 marker) compared with all other groups after 3 and 7 days of treatment (Fig. 7D–H and Fig. S16). That is, the wounds were still in the inflammatory phase of healing. In contrast, different degrees of reduction in wound tissue inflammation were observed in the ACG-GC/SPS, ACG-GC/Reu, and ACG-GC/Reu/SPS groups, suggesting that wound healing in these groups had already progressed beyond the inflammatory phase and entered the post-inflammatory phase. The extent of inflammation reduction was in descending order: ACG-GC/SPS < ACG-GC/Reu < ACG-GC/Reu/SPS. These results indicate that the ACG-GC/Reu/SPS hydrogel alleviates inflammatory response by inducing the transformation of macrophage from the pro-inflammatory to the anti-inflammatory phenotype. The therapeutic effects of the ACG-GC/Reu/SPS hydrogel, which may be attributed to the presence and release of Reu and SPS. Release of these factors endowed the hydrogel with excellent anti-inflammatory, immunoregulatory and anti-inflammatory properties. This makes the GC/Reu/SPS hydrogel effective in preventing wound infections, shortening the inflammatory period of wound healing, and promoting wound healing.

Neovascularization promotes fibroblast migration and proliferation, collagen deposition, and re-epithelialization through the transportation of oxygen and nutrients to the wound sites. As shown in Fig. S17, immunofluorescent staining results indicated that the wounds treated with the ACG-GC/Reu/SPS hydrogel presented significantly higher level of CD31 and α-SMA on day 7 than the Control, ACG-GC, ACG-GC/SPS, and ACG-GC/Reu groups. Besides, the expression of CK14 in the ACG-GC/Reu/SPS group was remarkably higher than the other groups (Fig. S18). These results indicate that the ACG-GC/Reu/SPS hydrogel can promote neovascular remodeling and epithelial proliferation, thereby accelerating wound healing.

We performed an ELISA assay for several key factors in the serum of wound model rats (Fig. S19) to assess the promotional effects of SPS and Reu on tissue regeneration. The results showed that the serum levels of

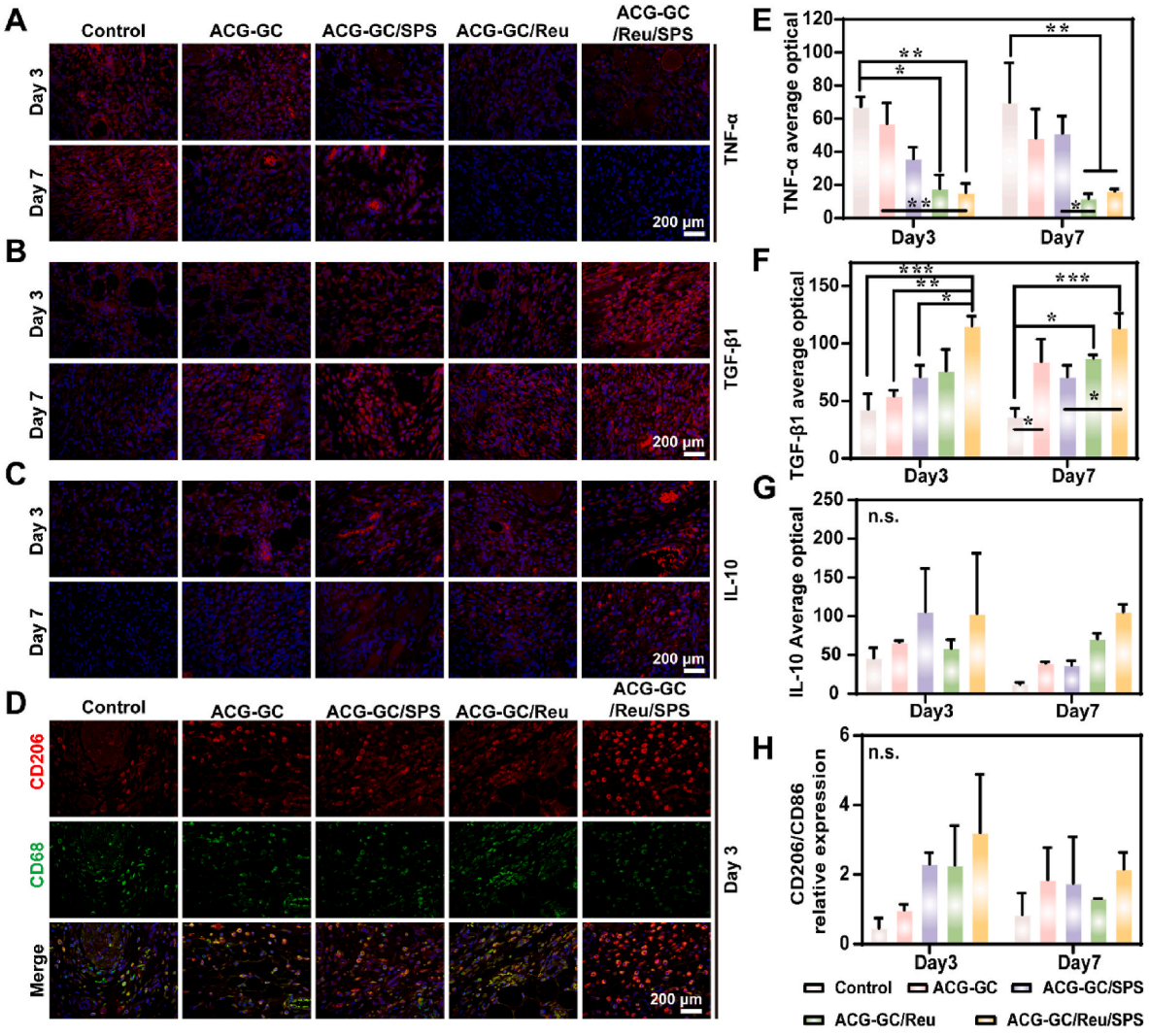

Fig. 7. ***In vivo*** **immunoregulatory and anti-inflammatory properties of the hydrogels in a total skin defect infection model of SD rats.**
Immunofluorescence staining of (A) TNF-α, (B) TGF-β1 and (C) IL-10 in the skin of the injury site after 3 and 7 days of treatment; (D) Immunofluorescence staining of CD206 (red) and CD86 (green) in macrophages after 3 days of treatment; Quantitative analyses of the positivity rates of (E) TNF-α, (F) TGF-β1 and (G) IL-10; (H) Analysis of relative CD206/CD86 expression.

FGF-1, ANG-1, VEGF and Collagan I were significantly higher in the SPS and Reu-treated group compared with the control group. This indicated that the synergistic effect of SPS and Reu not only contributed to macrophage polarization, but also further accelerated wound healing by promoting neovascularization and collagen deposition.

To evaluate the biocompatibility of tissues after hydrogel treatment. We performed HE staining of the tissue structures of the heart, liver, spleen, lungs, and kidneys of the treated rats (Fig. S20). The tissues in the Control group showed some minor structural abnormalities, but no obvious tissue damage was seen. All tissues in the hydrogel-treated group showed better tissue structure with no obvious cellular damage or inflammatory reaction. This suggests that the hydrogel caused no significant toxicity or damage to the major organs of the rats. Meanwhile, blood parameters were assessed in the blood of rats after 14 days of treatment (Fig. S21), and all hydrogel-treated groups showed less changes in hematological indices compared with the control group, and no significant abnormalities were observed. The above results indicated that the hydrogel was biocompatible *in vivo*.

2.6. *In vitro and in vivo real-time temperature monitoring capabilities*

Temperature is a critical indicator in the healing of infected wounds, reflecting the inflammation and healing status [52,53]. To evaluate its potential as monitoring devices, the temperature sensing property of the ACG-GC/Reu/SPS-PDMS hydrogel was tested. Firstly, the hydrogel was placed in a temperature-controlled box and the transmission spectra at various temperatures were recorded. As shown in Fig. 8A, the results showed that the designed hydrogel has an excellent temperature sensitivity (defined as $S = \Delta\lambda/\Delta T$, where $\Delta\lambda$ is the drift of the Bragg wavelength, and ΔT is the change in temperature) and it is suitable for further testing. Meanwhile, Fig. S22 showed that the Bragg wavelength drift correlates linearly with temperature changes between 34 and 43 °C. Furthermore, Fig. 8B illustrated that the Bragg wavelength shifted toward the longer wavelengths as the temperature increased from 36.5 °C to 38.5 °C. This observation is indicative of a fast response speed and real-time temperature recording capacity. As shown in Fig. 8C, a warming-cooling cycle was conducted to examine the reversibility of the response of the hydrogel to temperature changes, and the hydrogel demonstrated good temperature reversibility. Temperature stability was also tested (Fig. 8D) and found to be reliable. These results indicate that the hydrogel has a fast response, excellent reversibility, and stability, and can continuously, accurately, and promptly monitor wound temperature changes.

Generally, the temperature of normal skin tissue is typically around 36 °C. In comparison, the temperature of bacterially infected wound tissue may be elevated. As the wound heals, the wound temperature gradually returns to normal levels [54]. Considering the complexity and diversity of the wound healing process, more pathological processes need to be investigated. Herein, wound infection served as a model of pathology during the wound-healing process and temperature was selected as one of the monitoring signs [55,56]. Based on the excellent temperature responsiveness of the ACG-GC/Reu/SPS-PDMS hydrogel *in vitro*, a total skin defect infection model in SD rats was used to test the ability of the ACG-GC/Reu/SPS-PDMS hydrogel to monitor temperature of the wound *in vivo*. The temperatures of the wound *in vivo* were monitored using a thermal camera (real temperature) and the hydrogel (testing temperature) (Fig. 8E and F). An increase in wound temperature after bacterial infection (day 0) was observed. This was followed by a steep drop in temperature after treatment with the hydrogel. The wound temperature subsequently returned to normal temperature levels. Although the temperature recorded by the hydrogel differed from the actual temperature of the infected wound as measured by the thermal camera, a consistent trend was shown. These results indicate the sensitivity and reliability of the hydrogel in monitoring wound healing progress. Therefore, our constructed ACG-GC/Reu/SPS-PDMS hydrogel provides an entirely new platform for overcoming the unknown status of the healing process.

2.7. *In vivo healing capability in a total skin defect infection model of Bama minipigs*

To further verify the therapeutic effect of the ACG-GC/Reu/SPS

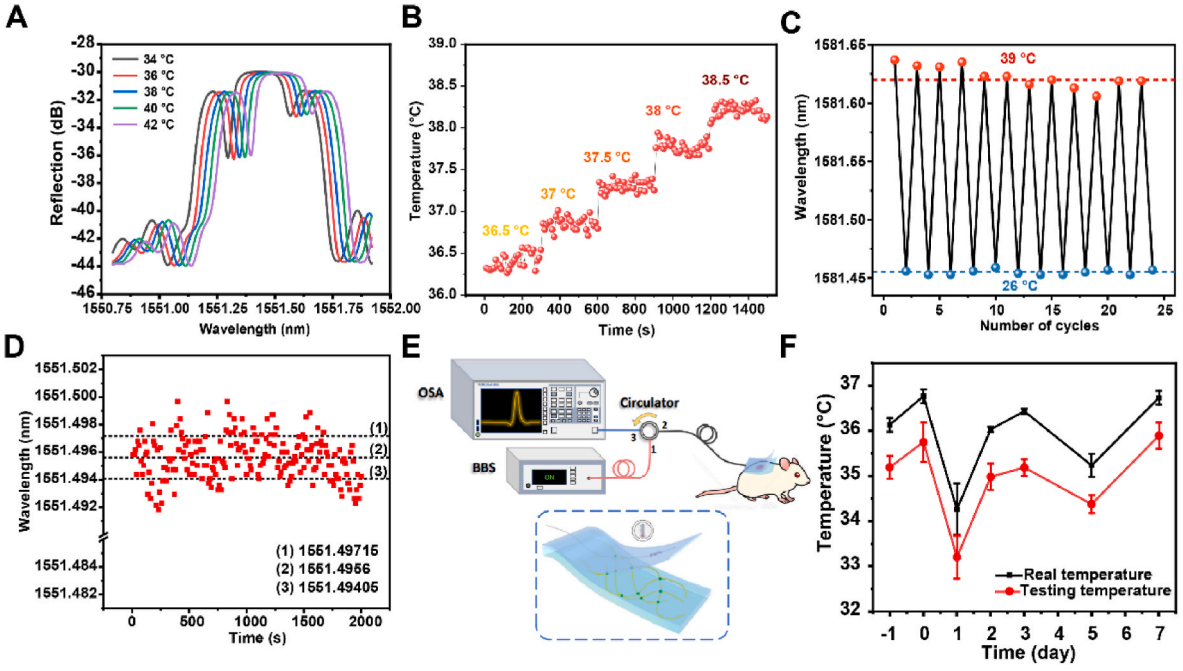

Fig. 8. *In vitro* and *in vivo* real-time temperature monitoring capability of the hydrogels.
(A) Transmission spectra of the temperature-sensitive optical fiber-ACG-GC/Reu/SPS hydrogel at different temperatures; (B) Real-time temperature information the hydrogel; (C) Reversibility test of temperature response and (D) Temperature stability test of the hydrogel; (E) Diagram illustrating the hydrogel working principle; (F) Temperature changes of the hydrogel at different time-points.

hydrogel on wound healing, we created a pig infected-wound model (Fig. 9A), since the skin of this animal has considerable similarity with that of the human [57]. The photographic record (Fig. 9B) and the general picture of wound healing (Fig. 9C) showed that wounds gradually healed with the increase in treatment time. By day 14 of treatment, the wounds in the hydrogel group exhibited obvious healing compared to the control group. By day 42, the wounds in the hydrogel group were almost completely healed. Further assessment of wound healing in Bama pigs involved histological measurements, including H&E and Masson staining of tissues from wound sites treated for 7, 21 and 42 days. Hematoxylin-eosin staining images at 7, 21, and 42 days of treatment were shown in Figs. S23A, S24A, and Fig. 9D, respectively. These images showed an inflammatory response in all groups. However, there was less inflammatory infiltration in wounds treated with the hydrogel. As the treatment time increased, the inflammatory response of the wounds gradually decreased, and more fibroblasts could be seen. Wounds treated with the ACG-GC/Reu/SPS hydrogel also demonstrated more follicular structures and neovascularization compared to the other groups. Masson staining images at 7, 21, and 42 days of treatment are shown in Fig. S23B, Fig. S24B, and Fig. 9E, respectively. The amount of collagen fibrils gradually increased with treatment time. Nevertheless, collagen deposition was always the highest in the hydrogel-treated wounds. The excellent antibacterial activity of the hydrogel prevented the wound from bacterial infections. This resulted in a reduction of inflammatory reactions and better healing of the infected wounds. Skin wound healing involves platelets, inflammatory cells, epithelial cells, keratinocytes, fibroblasts, various cytokines, growth factors, and other biologically active molecules. Interaction mediated by integrin receptor and adhesion molecule with extracellular matrix components are also essential [58]. Throughout this process, transforming growth factor β1 (TGF-β1) and interleukin-10 (IL-10) play crucial roles in inflammatory and reparative phases. These cytokines regulate epithelialization, collagen accumulation, and angiogenesis [59]. Immunofluorescence staining was performed on tissue samples harvested from wound sites during treatment to examine the expression of TGF-β1 and IL-10 on day 21 (Fig. S25A) and 42 (Fig. 9F) of treatment. In addition, the expression levels of TGF-β1 and IL-10 were quantified on day 21 (Fig. S25B), and on day 42 for TGF-β1 (Fig. 9G) and IL-10 (Fig. 9H). The highest expressions of TGF-β1 and IL-10 was observed in the hydrogel group. This indicates that treatment with the ACG-GC/Reu/SPS hydrogel reduced the inflammatory response of the wound. Adhesion spot kinase (FAK) is a non-receptor tyrosine kinase that normally transduces cell adhesion signals to regulate various biological cellular functions such as cell survival, migration, and cancer cell invasion [54–56]. Staining of the GC/Reu/SPS hydrogel group with FAK demonstrated down-regulated FAK expression, which could inhibit tumor cell proliferation, migration, and invasion (Fig. 9F–I). In addition, the expression of intracellular phosphatidylinositol kinase (PI3K) was down-regulated in the same treatment group (Fig. 9F–J). This was associated with reduced apoptosis and enhanced cell survival and proliferation.

To find out how the ACG-GC/Reu/SPS-PDMS hydrogel promotes infected wound healing, RNA sequencing (RNA-Seq) analysis was performed in a total skin defect infection model of Bama minipigs. Compared to the control group (without treatment), 120 differentially expressed genes (DEGs) were found in the test (treatment by the ACG-GC/Reu/SPS-PDMS hydrogel) group and shown in the cluster heatmap, including 109 up-regulated genes and 11 down-regulated genes (Fig. 10A and B). The chord plot in Fig. 10C showed the down-regulated genes and their corresponding GO biological processes, such as inflammatory responses, immune system processes and immune responses. Fig. 10D is a heatmap depicting the expression patterns of 120 DEGs between the control and test groups. The Gene Ontology (GO) enrichment analysis of these DEGs covered biological processes, cellular components, and molecular functions (Fig. 10E). To gain insight into the signaling pathways activated by the ACG-GC/Reu/SPS-PDMS hydrogel, the relevant signaling pathways were explored using gene set enrichment analysis (GSEA) (Fig. 10F). The results showed down-regulation of AMPK, IL-17, NF-kappa β signaling pathways and activation of NLRP3 inflammasome in wound tissues treated with the ACG-GC/Reu/SPS-PDMS hydrogel. Kyoto Encyclopedia of Genes and Genomes (KEGG) pathway enrichment analysis confirmed the MAPK, TGF-β, PI3K-Akt, TNF, VEGF signaling pathway plays an important role (Fig. 10G). Among them, FAK and PI3K/Akt signaling pathways play important roles in cell survival, proliferation, migration, and angiogenesis. FAK promotes cell migration and proliferation by regulating cell-substrate interactions, thereby accelerating the wound repair process. Meanwhile, by regulating the activity of Akt, PI3K not only promoted cell proliferation and survival, but also activated angiogenesis-related signaling pathways, contributing to wound vascular regeneration and repair. The complementary and synergistic effects of FAK and PI3K pathways may be an important mechanism by which the hydrogel material promotes wound healing in this study.

2.8. In vivo healing and wound closure capabilities in a full-thickness skin incision model of Bama minipigs

The results mentioned above demonstrated that the hydrogel with excellent tissue adhesion capacity, accelerated hemostatic ability and good biocompatibility could be a promising candidate for suture less wound closure. A full-thickness skin incision of 40 mm was created on the back of Bama minipigs after anesthesia to reduce the influence of individual differences on the results. Those incisions were closed by suture (Suture group) and the ACG hydrogel (ACG group), and exposure without any treatment was set as the Control group. As shown in Fig. S26A, photographs of the wounds showed different healing stages and morphologies at postoperative days 7, 14, 21, and 42. The incisions treated by the ACG hydrogel showed better closure than that treated by suture or that without any intervention. The wound became larger at the very beginning due to the movement of the minipig, which delayed the healing process. Although the incisions are well closed by suture, the scar, redness and certain damage caused by suture could not be ignored. On day 21, the incision closed with the hydrogel is almost healed, while obvious wounds still remain in the incisions without treatment or treated by suture. These results are indicative of an effective wound closure effect of the hydrogel. Histological analysis was performed to further evaluate the healing effect of the closed incisions on day 7, 21 and 42. Results from H&E staining showed that the wounds treated with the hydrogel showed less inflammatory cell infiltration than the Control and suture groups (Fig. S26B). Masson's trichrome staining results demonstrated that more cellular infiltration, extracellular matrix secretion, and neovascularization in the hydrogel group indicated better post-wound-closure care (Fig. S26C). In addition, immunofluorescent staining results showed that less FAK and PI3K expression was found in the hydrogel group than the other groups (Figs. S26D and S26E). These results suggest that the hydrogel with high adhesive strength and good biocompatibility could well close the incision and promote the healing of wounds [60].

3. Conclusion

In summary, we validated the efficacy of a strategy of "sense-and-treat" and our constructed GC/Reu/SPS-PDMS hydrogel in the context of biomedical applications. The integration of bacterio-therapeutics and bio-optics provides an entirely new platform for developing smart, real-time diagnostics and timely wound treatment. The value of wound temperature changes can be monitored in real-time by this hydrogel quickly and accurately. The capability to track temperature changes provides an effective and timely reference basis for wound management. What's more, through the transcriptomic analysis (RNA-Seq) carried out in the Parma minipig model, we have deeply revealed the regulatory effects of this hydrogel on key signaling pathways (including down-regulation of pathways such as AMPK, IL-17, and NF-κB, and

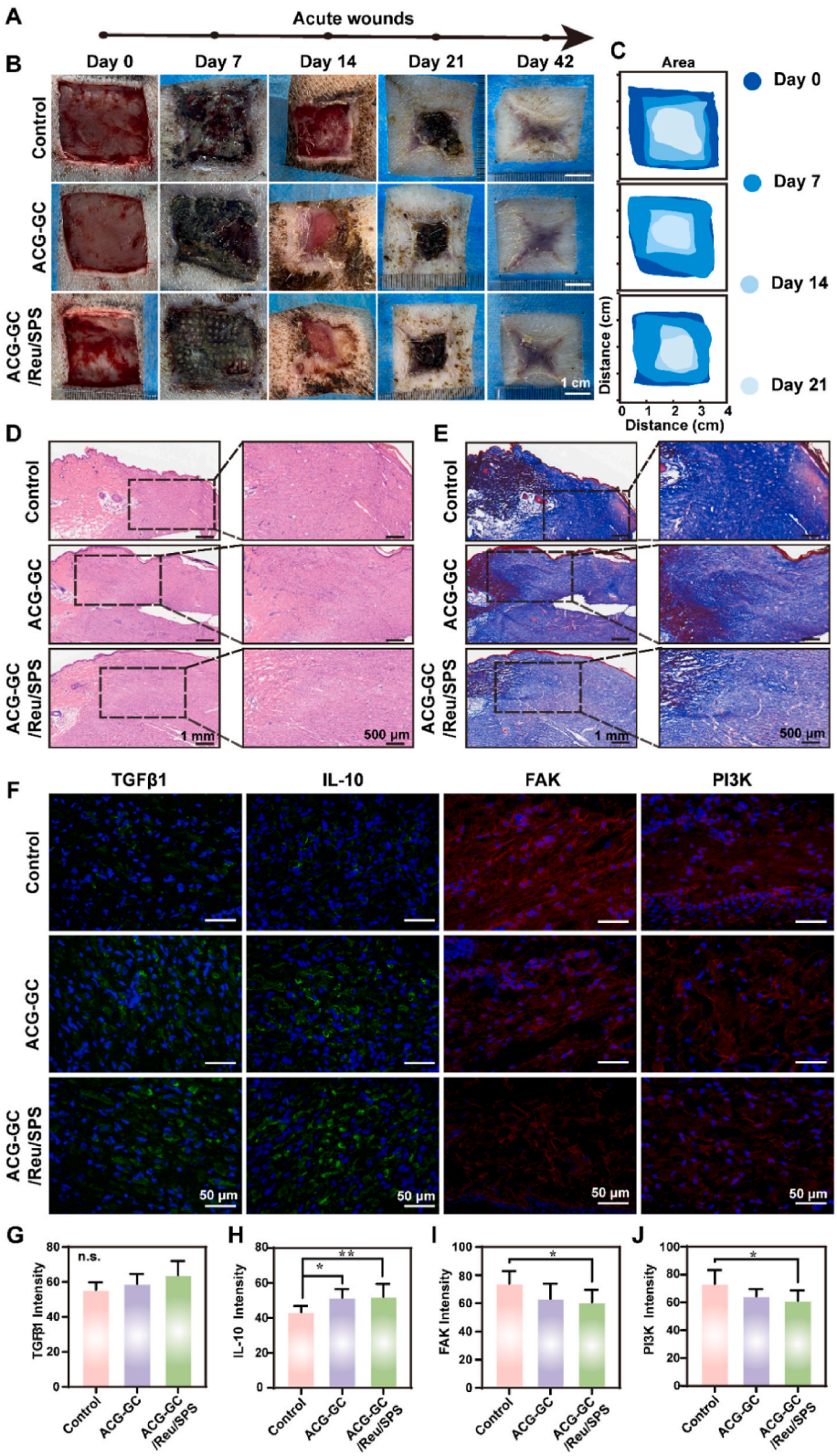

Fig. 9. ***In vivo*** **healing capability of the hydrogels in a total skin defect infection model of Bama minipigs.**
(A) Overview of the formation of a model of a whole-layer infected skin defect in the Bama pig and the time-point of treatment; (B) Macroscopic images of wounds at corresponding time-points (days 0, 7, 14, 21, and 42); (C) Representative images of wound healing at days 0, 7, 14, 21, and 42 after different treatments; (D) H&E and (E) Masson's trichrome staining of tissue at the wound site on day 42 of treatment; (F) TGF-β1, IL-10, FAK, PI3K staining of the wound on day 7; Quantitative analyses of (G) TGF-β1, (H) IL-10, (I) FAK and (J)PI3K expression.

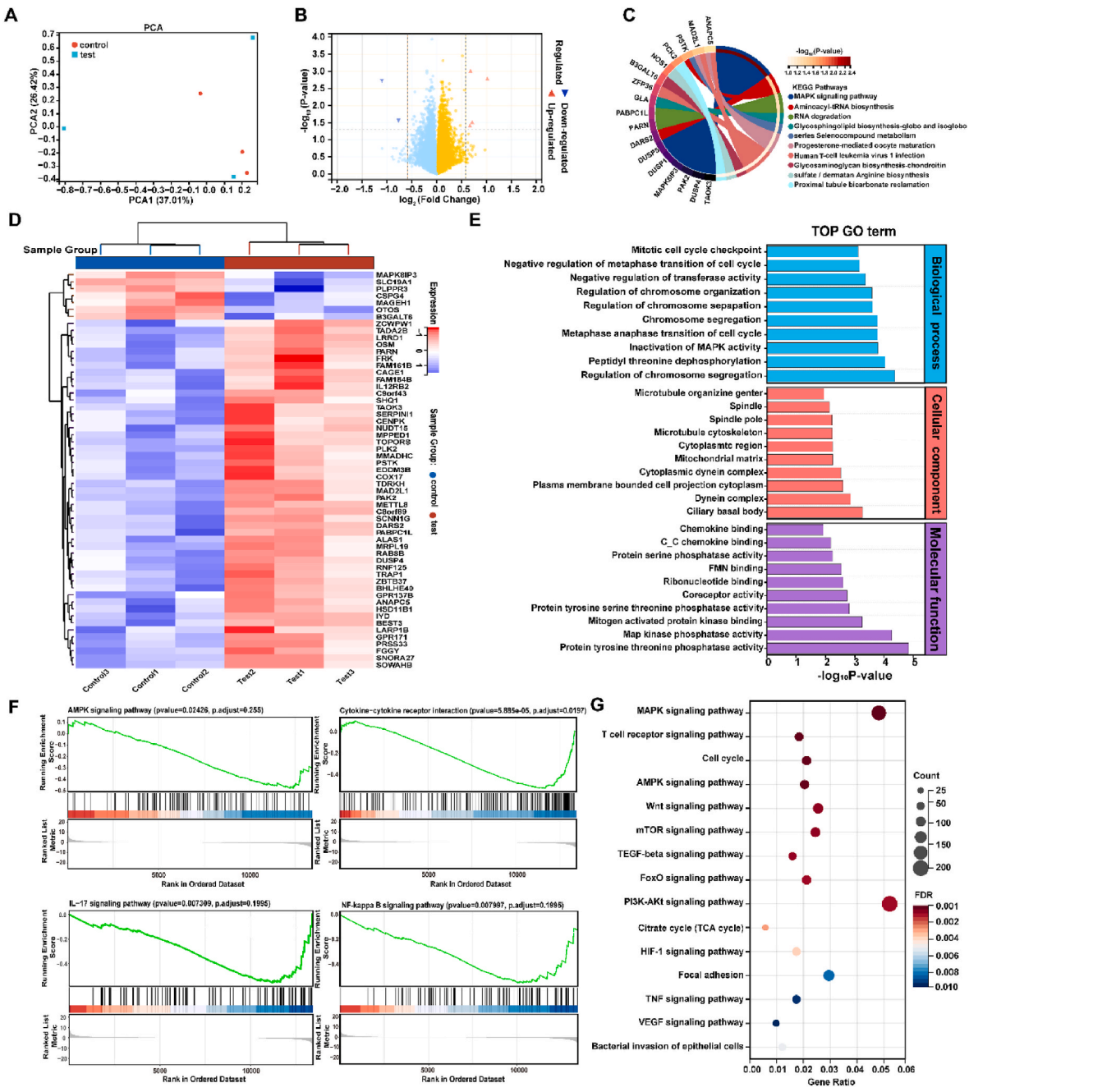

Fig. 10. Analysis of RNA sequencing.
(A) PCA analysis presenting differentially expressed genes (DEGs) identified by RNA-seq in control and test groups; (B) Volcano diagram illustrating DEGs (red indicates up-regulated genes; blue represents down-regulated genes); (C) String diagram showing gene ontology-enriched terms and their corresponding top 10 down-regulated genes; (D) Heatmap representation of DEGs; (E) Gene ontology enrichment analysis presenting DEGs; (F) GSEA showing DEGs within the KEGG pathway; (G) Differential gene enrichment analysis within the KEGG pathway.

activation or enrichment of pathways such as MAPK, TGF-β, PI3K-Akt, TNF, and VEGF), which can play an active role in cellular immunomodulation, angiogenesis and tissue regeneration. This study provides strong evidence to further understand the molecular mechanism of the hydrogel in promoting wound healing, and also indicates that the hydrogel has high potential for clinical translation.

CRediT authorship contribution statement

Longbao Feng: Conceptualization. **Qing Peng:** Formal analysis. **Li Miao:** Data curation. **Chenghao Cai:** Resources. **Franklin R. Tay:** Visualization. **Shuqin Zhou:** Methodology. **Ying Zhang:** Software. **Zonghua Liu:** Supervision, Conceptualization. **Xingang Wang:** Project administration, Conceptualization. **Yang Jiao:** Project administration, Methodology. **Rui Guo:** Supervision.

Ethics approval and consent to participate

All animal handling protocols and experiments were approved by Institutional Animal Care and Use Committee of Ruige Biotechnology (Approval NO. 20220301011), and adhered to the National Institutes of Health Guide for the Care and Use of Laboratory Animals.

Declaration of competing interest

The authors declare that they have no known competing financial interests or personal relationships that could have appeared to influence the work reported in this paper.

Acknowledgements

This work was supported by This study was supported financially by the National Key Research and Development Program of China (No. 2022YFE0122200, No. 2022YFC2403102), the Marine Economy Development Project of Department of Natural Resources of Guangdong Province (No. GDNRC[2023]35), the Science and Technology Project of Guangdong Province (No. 2022A0505050046), the Key Areas and Development Program of Guangdong Province (No. 2020B1111560001, No. 2022B1111080007), the Key Areas and Development Program of Guangzhou (No. 202103030003, No. 2024B03J1244), the International Science and Technology Cooperation Project of Huangpu District/ Guangzhou Development District (No. 2021GH16), and the Project Team of Foshan National Hi-tech Industrial Development Zone Industrialization Entrepreneurial Teams Program (2320197001409), the Beijing Natural Science Foundation (No. 7242279), the National Natural Science Foundation of China (No. 82101069), the Beijing Nova Program (No. 20230484283), the Beijing Municipal Science & Technology Commission (No. Z221100007422130) and the Youth Incubation Program of Medical Science and Technology of PLA (No. 21QNPY116).

Appendix A. Supplementary data

Supplementary data to this article can be found online at https://doi.org/10.1016/j.bioactmat.2025.02.001.

References

[1] G.C. Gurtner, S. Werner, Y. Barrandon, et al., Wound repair and regeneration, Nature 453 (7193) (2008) 314–321.
[2] Z. Wu, W. Zhou, W. Deng, et al., Antibacterial and hemostatic thiol-modified chitosan-immobilized agnps composite sponges, ACS Appl. Mater. Interfaces 12 (18) (2020) 20307–20320.
[3] I. Sultan, S. Rahman, A.T. Jan, et al., Antibiotics, resistome and resistance mechanisms: a bacterial perspective, Front. Microbiol. 9 (2018) 2066.
[4] S. Rawal, S.A. Ali, Probiotics and postbiotics play a role in maintaining dermal health, Food Funct. 14 (9) (2023) 3966–3981.
[5] Y. Liang, X. Zhao, T. Hu, et al., Mussel-inspired, antibacterial, conductive, antioxidant, injectable composite hydrogel wound dressing to promote the regeneration of infected skin, J. Colloid Interface Sci. 556 (2019) 514–528.
[6] M.S. Refat, K.M. Elsabawy, A. Alhadhrami, et al., Development of medical drugs: synthesis and in vitro bio-evaluations of nanomedicinal zinc–penicillins polymeric hydrogel membranes for wound skin dressing by new chemical technology, J. Mol. Liq. 255 (2018) 462–470.
[7] R. Rakhshaei, H. Namazi, A potential bioactive wound dressing based on carboxymethyl cellulose/zno impregnated mcm-41 nanocomposite hydrogel, Mater. Sci. Eng. C 73 (2017) 456–464.
[8] B. Singh, S. Sharma, A. Dhiman, Design of antibiotic containing hydrogel wound dressings: biomedical properties and histological study of wound healing, Int. J. Pharm. 457 (1) (2013) 82–91.
[9] Y. Liu, Y. Sui, C. Liu, et al., A physically crosslinked polydopamine/nanocellulose hydrogel as potential versatile vehicles for drug delivery and wound healing, Carbohydr. Polym. 188 (2018) 27–36.
[10] S. McMahon, R. Kennedy, P. Duffy, et al., Poly(Ethylene glycol)-based hyperbranched polymer from raft and its application as a silver-sulfadiazine-loaded antibacterial hydrogel in wound care, ACS Appl. Mater. Interfaces 8 (40) (2016) 26648–26656.
[11] W. Zheng, H. Shen, Y. Cheng, et al., Au nanorods activate Zn^{2+}/Ag^{+} mediated anti-inflammatory for enhanced methicillin-resistant wound repair via bionic claw microneedles, ACS Mater. Lett. 6 (10) (2024) 4791–4800.
[12] L.T. Axelsson, T.C. Chung, W.J. Dobrogosz, et al., Production of a broad spectrum antimicrobial substance by Lactobacillus reuteri, Microb. Ecol. Health Dis. 2 (2) (1989) 131–136.
[13] M.-C. Sun, Z.-Y. Hu, D.-D. Li, et al., Application of the reuterin system as food preservative or health-promoting agent: a critical review, Foods 11 (24) (2022) 4000.
[14] T.L. Talarico, W.J. Dobrogosz, Chemical characterization of an antimicrobial substance produced by Lactobacillus reuteri, Antimicrob. Agents Chemother. 33 (5) (1989) 674–679.
[15] L. Schaefer, T.A. Auchtung, K.E. Hermans, et al., The antimicrobial compound reuterin (3-hydroxypropionaldehyde) induces oxidative stress via interaction with thiol groups, Microbiology 156 (6) (2010) 1589–1599.
[16] O. Eskilson, E. Zattarin, L. Berglund, et al., Nanocellulose composite wound dressings for real-time ph wound monitoring, Mater. Today bio. 19 (2023) 100574.
[17] X. Xiao, X. Xiao, A. Nashalian, et al., Triboelectric nanogenerators for self-powered wound healing (adv. Healthcare mater. 20/2021), Adv. Healthcare Mater. 10 (20) (2021) 2170097.
[18] P. Mostafalu, A. Tamayol, R. Rahimi, et al., Smart bandage for monitoring and treatment of chronic wounds, Small 14 (33) (2018) 1703509.
[19] M.S. Brown, B. Ashley, A. Koh, Wearable technology for chronic wound monitoring: current dressings, advancements, and future prospects, Front. Bioeng. Biotechnol. 6 (2018).
[20] Y. Gao, D.T. Nguyen, T. Yeo, et al., A flexible multiplexed immunosensor for point-of-care in situ wound monitoring, Sci. Adv. 7 (21) (2023) eabg9614.
[21] Y. Zhang, Y. Hu, Y. Montelongo, et al., A conformable holographic sensing bandage for wound monitoring, Adv. Funct. Mater. 34 (16) (2024) 2308490.
[22] A. Leal-Junior, J. Guo, R. Min, et al., Photonic smart bandage for wound healing assessment, Photon. Res. 9 (3) (2021) 272–280.
[23] H. Bai, S. Li, J. Barreiros, et al., Stretchable distributed fiber-optic sensors, Science 370 (6518) (2020) 848–852.
[24] Y. Min, R. Han, G. Li, et al., The ph-sensitive optical fiber integrated cmcs-Pa@Fe hydrogels for photothermal therapy and real-time monitoring of infected wounds, Adv. Funct. Mater. 33 (16) (2023) 2212803.
[25] Y. Li, C. Zheng, S. Liu, et al., Smart glove integrated with tunable mwnts/pdms fibers made of a one-step extrusion method for finger dexterity, gesture, and temperature recognition, ACS Appl. Mater. Interfaces 12 (21) (2020) 23764–23773.
[26] Z. Shentu, J. Kang, Z. Zhu, et al., No-core pdms fiber for large-scale strain and concentration measurement, Opt. Fiber Technol. 63 (2021) 102531.
[27] S. Correa, A.K. Grosskopf, H. Lopez Hernandez, et al., Translational applications of hydrogels, Chem. Rev. 121 (18) (2021) 11385–11457.
[28] D. Buenger, F. Topuz, J. Groll, Hydrogels in sensing applications, Prog. Polym. Sci. 37 (12) (2012) 1678–1719.
[29] Q. Zhang, X. Zhou, H. Du, et al., Bifunctional hydrogel-integrated 3d printed scaffold for repairing infected bone defects, ACS Biomater. Sci. Eng. 9 (8) (2023) 4583–4596.
[30] X. Zhou, Y. Qian, L. Chen, et al., Flowerbed-inspired biomimetic scaffold with rapid internal tissue infiltration and vascularization capacity for bone repair, ACS Nano 17 (5) (2023) 5140–5156.
[31] Y. Wang, J. Wang, R. Gao, et al., Biomimetic glycopeptide hydrogel coated Pcl/Nha scaffold for enhanced cranial bone regeneration via macrophage M2 polarization-induced osteo-immunomodulation, Biomaterials 285 (2022) 121538.
[32] T. Chen, Y. Chen, H.U. Rehman, et al., Ultratough, self-healing, and tissue-adhesive hydrogel for wound dressing, ACS Appl. Mater. Interfaces 10 (39) (2018) 33523–33531.
[33] C. Xuan, L. Hao, X. Liu, et al., Wet-adhesive, haemostatic and antimicrobial bilayered composite nanosheets for sealing and healing soft-tissue bleeding wounds, Biomaterials 252 (2020) 120018.
[34] Y. Yang, X. Zhao, J. Yu, et al., Bioactive skin-mimicking hydrogel band-aids for diabetic wound healing and infectious skin incision treatment, Bioact. Mater. 6 (11) (2021) 3962–3975.
[35] D. Deng, X. Li, J.-J. Zhang, et al., Biotin–avidin system-based delivery enhances the therapeutic performance of Msc-derived Exosomes, ACS Nano 17 (9) (2023) 8530–8550.
[36] X. Zhang, X. Zhan, C. Hu, et al., Light-controlled crosslinked multifunctional "Band-Aids" as dual-stage wound dressing for dynamic wound closure, Collagen and Leather 6 (1) (2024) 23.
[37] Z. He, Z. Zhou, W. Yuan, Highly adhesive, stretchable, and antifreezing hydrogel with excellent mechanical properties for sensitive motion sensors and temperature-/humidity-driven actuators, ACS Appl. Mater. Interfaces 14 (33) (2022) 38205–38215.
[38] G. Bao, T. Jiang, H. Ravanbakhsh, et al., Triggered micropore-forming bioprinting of porous viscoelastic hydrogels, Mater. Horiz. 7 (9) (2020) 2336–2347.
[39] Y. Liang, H. Xu, Z. Li, et al., Bioinspired injectable self-healing hydrogel sealant with fault-tolerant and repeated thermo-responsive adhesion for sutureless post-wound-closure and wound healing, Nano-Micro Lett. 14 (1) (2022) 185.
[40] H.N. Wilkinson, M.J. Hardman, Wound healing: cellular mechanisms and pathological outcomes, Open Biology 10 (9) (2020) 200223.
[41] J. Yang, Z. Chu, Y. Jiang, et al., Multifunctional hyaluronic acid microneedle patch embedded by cerium/zinc-based composites for accelerating diabetes wound healing, Adv. Healthcare Mater. 12 (24) (2023) 2300725.
[42] V.H. Urrutia-Baca, E. Escamilla-García, M.A. de la Garza-Ramos, et al., In vitro antimicrobial activity and downregulation of virulence gene expression on Helicobacter pylori by reuterin, Probiot. Antimicrobial Proteins 10 (2) (2018) 168–175.
[43] H.-F. Liang, C.-N. Chen, Y. Chang, et al., Natural antimicrobial agent (reuterin) produced by Lactobacillus reuteri for sanitization of biological tissues inoculated with Pseudomonas aeruginosa, Biotechnol. Bioeng. 84 (2) (2003) 233–239.
[44] V. Rosa, N. Silikas, B. Yu, et al., Guidance on the assessment of biocompatibility of biomaterials: fundamentals and testing considerations, Dent. Mater. 40 (11) (2024) 1773–1785.
[45] L. Yang, F. Liang, X. Zhang, et al., Remodeling microenvironment based on mofs-hydrogel hybrid system for improving diabetic wound healing, Chem. Eng. J. 427 (2022) 131506.

[46] D. Hirayama, T. Iida, H. Nakase, The phagocytic function of macrophage-enforcing innate immunity and tissue homeostasis, Int. J. Mol. Sci. 19 (1) (2018) 92.
[47] A. Shapouri-Moghaddam, S. Mohammadian, H. Vazini, et al., Macrophage plasticity, polarization, and function in health and disease, J. Cell. Physiol. 233 (9) (2018) 6425–6440.
[48] S.-K. Han, Basics of wound healing, in: Innovations and Advances in Wound Healing, 2023, pp. 1–42.
[49] S. Pourshahrestani, E. Zeimaran, N.A. Kadri, et al., Polymeric hydrogel systems as emerging biomaterial platforms to enable hemostasis and wound healing, Adv. Healthcare Mater. 9 (20) (2020) 2000905.
[50] M. Li, Z. Zhang, Y. Liang, et al., Multifunctional tissue-adhesive cryogel wound dressing for rapid nonpressing surface hemorrhage and wound repair, ACS Appl. Mater. Interfaces 12 (32) (2020) 35856–35872.
[51] H. Chen, L. Wu, T. Wang, et al., Ptt/pdt-induced microbial apoptosis and wound healing depend on immune activation and macrophage phenotype transformation, Acta Biomater. 167 (2023) 489–505.
[52] D. Lou, Q. Pang, X. Pei, et al., Flexible wound healing system for pro-regeneration, temperature monitoring and infection early warning, Biosens. Bioelectron. 162 (2020) 112275.
[53] P. Salvo, V. Dini, A. Kirchhain, et al., Sensors and biosensors for C-reactive protein, temperature and ph, and their applications for monitoring wound healing: a review, Sensors 17 (12) (2017) 2952.
[54] H. Haidari, K. Vasilev, A.J. Cowin, et al., Bacteria-activated dual ph- and temperature-responsive hydrogel for targeted elimination of infection and improved wound healing, ACS Appl. Mater. Interfaces 14 (46) (2022) 51744–51762.
[55] J.R. Barzilay, R.N. Salas, J. Hess, et al., Overview of heat-related illnesses, N. Engl. J. Med. 390 (24) (2024) e63.
[56] H. Chen, J. Xu, J. Sun, et al., Recent advances on thermosensitive hydrogels-mediated precision therapy, Asian J. Pharm. Sci. 19 (3) (2024) 100911.
[57] J.K. Lunney, A. Van Goor, K.E. Walker, et al., Importance of the pig as a human biomedical model, Sci. Transl. Med. 13 (621) (2021) eabd5758.
[58] S. Mandla, L. Davenport Huyer, M. Radisic, Review: multimodal bioactive material approaches for wound healing, APL Bioeng. 2 (2) (2018) 021503.
[59] S.A. Eming, P. Martin, M. Tomic-Canic, Wound repair and regeneration: mechanisms, signaling, and translation, Sci. Transl. Med. 6 (265) (2014) 265sr6, 265sr6.
[60] Z. Yang, R. Huang, B. Zheng, et al., Highly stretchable, adhesive, biocompatible, and antibacterial hydrogel dressings for wound healing, Adv. Sci. 8 (8) (2021) 2003627.